Experimental Investigation of Piston-Free Expander Accompanied by Cold Linear Compressor

J. Park, S. Jeong

Cryogenic Engineering Laboratory, Mechanical Engineering Dept.,
School of Mechanical and Aerospace Engineering,
Korea Advanced Institute of Science and Technology, Daejeon, Korea

ABSTRACT

This research focuses on the study of a Stirling-type pulse tube refrigerator (PTR) designed to operate with a cold compressor, where 'cold' means much colder than ambient room temperature including cryogenic operating temperatures. Thus, the PV power is directly generated at a cryogenic temperature and transmitted to the cold expansion volume without undergoing a separate precooling process. Implementing a cold reservoir as a heat rejecter and regulating the entire operating temperature range of the PTR under sub-ambient temperature will enable the PTR to operate efficiently in cold environments like space.

As a proof of concept, this experimental investigation was conducted with a cold linear compressor operating at 80 K; whereby a no-load temperature of 18.7 K was achieved. The PTR including the cold linear compressor is expected to be further optimized at the system level for operation between 80 K and 20 K at the resonant state. This paper describes both preliminary test results and further discussions for an 'optimized' PTR system.

WHY DO WE FOCUS ON COLD COMPRESSION?

The main reason for cold compression is to improve compression efficiency and to get a 'lower temperature' at the cold expansion space. In order to get a 'lower temperature', many researchers have worked towards cascade pulse tube refrigerators (PTRs) introducing a precooling stage [1-3] or multistage cooling [4, 5]. Let us imagine that the pressure-volume work (PV work) is generated at a 'cold (sub-ambient temperature)' state. As the thermodynamic state of the working gas becomes close to its saturation curve, the specific volume decreases and incompressibility increases. The work consumption rate is represented by the following equation [6]:

$$\dot{W}_{PdV} = \int P dv \tag{1}$$

The reduced specific volume of the working gas enables the work consumption in pressurizing it to be decreased. The generated PV work is then transmitted to a 'colder' state with a precooling process. The work reduction due to the compression temperature ratio to the temperature where the working gas expands, is much smaller relative to that of a typical ambient-temperature Stirling-type PTR. This fact implies that the available mechanical work (PV work) transmitted to the expansion volume

Cryocoolers 19, edited by S.D. Miller and R.G. Ross, Jr.

is effectively convertible to increased cooling. Therefore, the cold-Stirling-type PTR can readily reach a lower target temperature with larger refrigeration potential than a typical ambient-temperature single-stage Stirling-type PTR. For a cold reservoir one can utilize the technically-mature liquefaction cycles widely-available in the gas liquefaction industry, i.e. liquefied natural gas (LNG), liquid nitrogen (LN_2) and liquid oxygen (LOX), etc. This concept can even be extended to liquid hydrogen (LH_2) and liquid helium (LHe) temperatures.

In order to implement a cold-Stirling-type PTR (or other regenerative-type refrigerator) for the large-scale gas industry, a fundamental investigation of the important characteristics must be carried out first [4, 7-9]. Finally, in the process of converting electrical to mechanical compression of the working gas, losses due to Joule heating are generated. When the linear compressor operates at a cryogenic temperature, it is possible to utilize high temperature superconductors (HTS) instead of typical metallic conductor coils for the linear motor. A cold compressor implemented with a HTS linear motor can intuitively eliminate the ohmic loss so that a higher motor efficiency can be expected. Nevertheless, since the heat generated due to the alternating current (AC) loss at cryogenic temperature generally creates significant burden, it has to be minimized for efficient motor operation. Several advantages of the 'cold compressor with piston-free cold expander' include:

(i) High density of the working gas; reducing compression work to the working gas
(ii) Cascade-like refrigeration system; increasing thermal efficiency
(iii) Superconducting enabling environment; increasing in electrical efficiency

In this paper, in order to demonstrate the concept of 'cold compression', a new cryogenically compatible linear compressor was developed. The cold linear compressor stably produces PV work around LN_2 temperature, and the efficiency of the electric input to the mechanical work conversion is estimated to exceed approximately 80% over a broad frequency range. As an expansion device, our pulsating tube was mated with a multilayered regenerator to widen the temperature span between the compression space where the PV work is generated and the cold-end where the working gas expands. At an operating frequency of 50 Hz, a lowest no-load temperature of 18.7 K was recorded. This paper also describes further investigations in two areas: first, to improve the resonance matching between the mechanical compressor and thermal efficiency needs of the cold end; this included a dynamic analysis of the whole PTR system with the commercial software (SAGE). The second investigation involved optimization of the multilayered regenerator with a sophisticated regenerator model (REGEN).

COLD LINEAR COMPRESSOR

As noted in Fig. 1, a 'single acting' and 'moving magnet' type linear compressor was developed for cryogenic temperature usage. The piston and the cylinder body were made of the same material (aluminum) and their surfaces were coated with Teflon. The piston has a 'gas bearing' to mitigate mechanical friction between the piston and the cylinder wall. We also installed a multi-flexure piston support (ASTM304) to maintain a neutral position of the piston. Radially magnetized permanent magnet segments were bonded with Stycast 2850FT epoxy on a stainless-steel guide that was mechanically connected with the piston. Inner and outer iron yokes were laminated for minimizing eddy current generation, and the inter gap between them was precisely adjusted to avoid conflict with the permanent magnet unit at cryogenic temperatures. We monitored the mean temperature in the compression space by installing a thermometer (DT-670, Lakeshore). In order to measure the effective mechanical power generated by the linear compressor, a dynamic pressure transducer (601A, Kistler) and an accelerometer (8730AE500M8, Kistler) were also mounted in the compression space and on the piston, respectively.

As noted in Fig. 1, all the compressor components including the electric coil were sealed in a hermetic stainless steel housing that was cooled by being submerged in liquid nitrogen (LN_2).

CRYOSTAT

The regenerator shell is 22.3 mm in diameter, 0.3 mm in thickness and 40 mm high. We selected a combination of stainless steel mesh screens (#400) and antimonial lead spheres ($Pb_{96}Sb_4$, 75 μm)

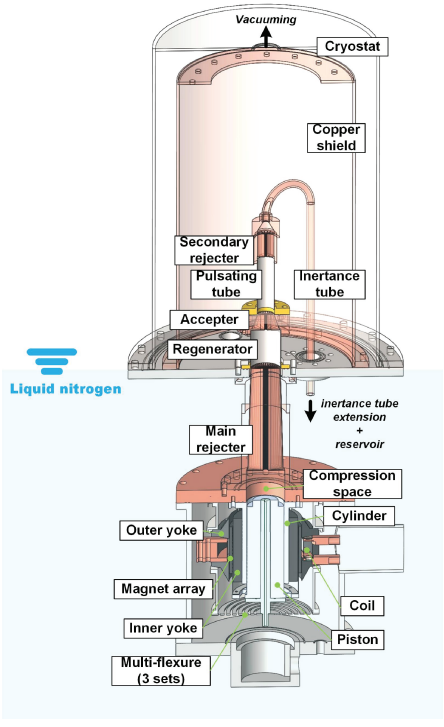

Figure 1. Rendering of the developed Stirling-type PTR system with its cold linear compressor.

after considering the thermal penetration depth of the working gas and of the regenerative material itself at the target operating temperatures. The lead spheres, with a filled length of 10 mm, were positioned nearest to the cold-end. Strictly speaking, the portion of each regenerative material in this first regenerator was a preliminary estimate, but had not yet been optimized. To provide for operational diagnostics, we attached E-type thermocouples on the outer surface of the regenerator shell (their opposite junctions were submerged in LN_2 for improved measurement accuracy). The thermocouples provide temperatures along the regenerator's axial direction that are useful to determine the effective thermal conduction through the matrix.

The pulsating tube canister (the pulse tube) is 12.7 mm in diameter, 0.3 mm in thickness, and 75 mm long. At the cold side of the pulsating tube and the regenerator, we installed an oxygen-free high conductivity (OFHC) copper cold-end heat exchanger (Accepter). Due to the difference in the tube diameters of the pulsating tube and the regenerator, it provided a smooth connection between them. To provide heat exchange surfaces, we carved several channels using electric discharge machining (EDM) within the copper. Other heat exchangers (main and secondary rejecters) also adopted this 'slit-type heat exchanger.' This 'slit-type heat exchanger' has several characteristics; it can have axisymmetric geometry with respect to the flowing direction, smooth channel connection, and no thermal contact resistance within the heat exchanger body. Nevertheless, it can create a flow maldistribution problem, so we installed flow straighteners at three locations of the PTR (at both ends of the pulsating tube and at the phase controller entrance) [10]. These consist of few layers of copper mesh screens (#200, totally 3 mm in thickness). The heat exchangers were designed and fabricated not to exceed a 1 K temperature difference between the working gas and the heat exchanger body at the corresponding target heat lift (100 W for the main heatsink rejector and 10 W for both the secondary heatsink rejector and the coldend heat exchanger) [11]. On the outer surfaces of both the coldend heat exchanger and the secondary heatsink, resistance thermometers (Cernox RTD, Lakeshore) were placed. An inertance tube (3.6 mm in inner diameter and 1.5 m in length) and a reservoir (volume of 500 cc) were connected in series to the secondary heatsink. A dynamic pressure trans-

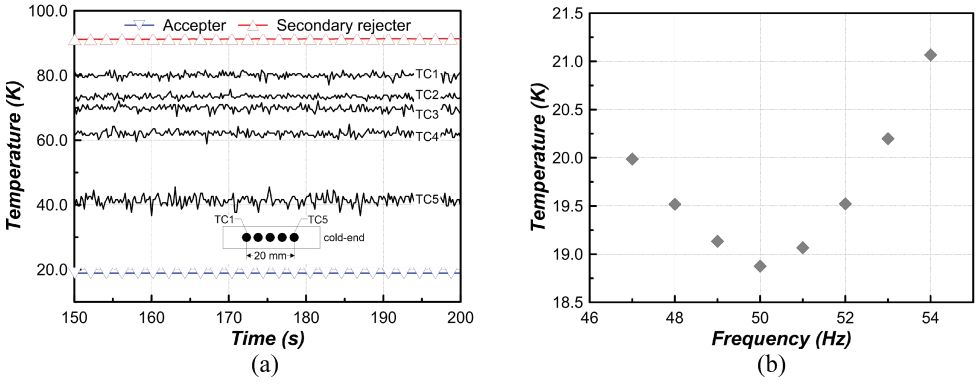

Figure 2. (a) Steady-state temperature distribution at a frequency of 50 Hz (b) frequency dependency of the coldend temperature (without thermal load).

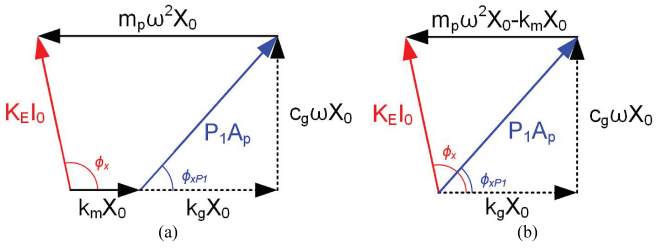

Figure 3. (a) Force phasor diagram of the linear compressor and (b) the modified one.

ducer (601A, Kistler) was also mounted to observe the pressure at the location where the working gas expands. A copper shield that was conductively cooled by LN_2 blocks thermal radiation to the cold parts. The secondary heatsink, moreover, was thermally connected to the copper shield by means of copper braid wires. All the cold parts are thermally insulated in vacuum with a copper radiation shield cooled by LN_2. The WHX, furthermore, is thermally anchored on the surface of the copper radiation shield by means of copper braid wires. We implemented a dynamic absorber to cancel the mechanical vibration that the single-acting piston generates. This consists of a flexure and a balancing mass that were manually tuned for the operating frequency.

EXPERIMENTAL RESULTS AND DISCUSSIONS

Figure 2(a) shows the temperature distribution at steady-state with the operating frequency of 50 Hz. In this case, a no-load temperature of 18.7 K was achieved, and it took 10 minutes to cool down from 80 K. Figure 2(b) shows the no-load temperature variation with the operating frequency.

In Figure 3(a), we introduce a force phasor diagram to determine the phase angle between the pressure and the piston displacement. Since the inertia and the spring force terms are in phase with each other, the phasor diagram can be simplified as depicted in Fig. 3(b). As we know the magnitudes of the physical variables as tabulated in Table 1, we can find the phase angle of the pressure relative to that of the piston displacement by applying the law of cosines. Consequently, we can evaluate the PV work in the compression space by using the following equation:

$$\dot{W}_{PdV1} = f\int P_1 dV = \pi f\left|P_1\right|\left|X_0\right|A_p \sin\left(\phi_{xP1}\right) \tag{2}$$

where, f is the operating frequency (Hz), P_1 is the dynamic pressure magnitude at the compression space (Pa), X_0 is the piston displacement (from the neutral position to its maximum peak, m), A_p is the cross-sectional area of the piston (m^2) and ϕ_{xP1} is the phase angle of the pressure relative to that of the piston displacement (°). Figure 4(a) shows the relative phase angle and the resultant PV power as estimated through the phasor analysis. Finally, we can claim that the cold linear compressor

Table 1. The measured physical variables and the pressure phase angle relative to that of the piston displacement and the corresponding PV work at the compression space

f (Hz)	X_0 (mm)	P_1 (kPa)	Analytically predicted from measured data with force phasor diagram	
			ϕ_{xP1} (°)	W_{PdV1} (W)
47	4.3	210.8	37.3	46.0
48	4.5	217.4	36.3	50.3
49	4.9	229.0	35.1	57.8
50	5.3	242.5	32.4	61.3
51	5.6	249.1	31.1	65.8
52	5.8	253.7	29.5	68.3
53	6.0	254.5	28.1	68.6
54	6.1	255.5	26.8	68.2

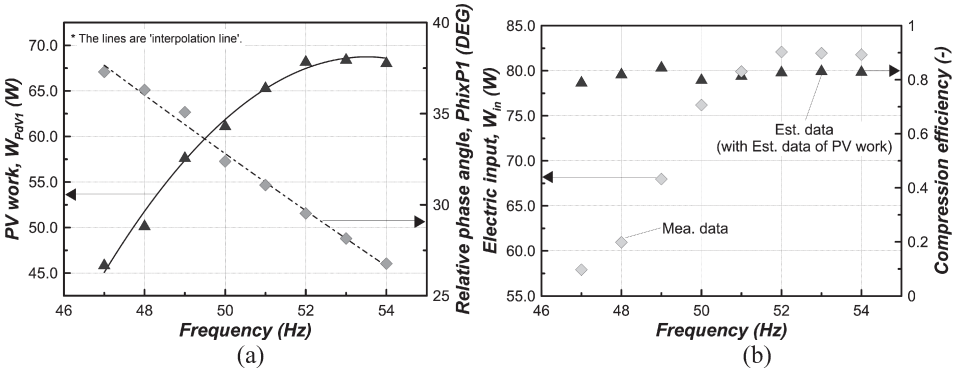

Figure 4. (a) The expected pressure phase angle relative to that of the piston displacement and the resultant PV work at the compression space and (b) the corresponding compression efficiency to the electric input.

stably generates PV power with the compression efficiency of over 80%, as represented in Fig. 4(b). The compression efficiency can be defined as the equation:

$$\eta_{comp.} = \frac{\dot{W}_{PdV1}}{\dot{W}_{in}} \tag{3}$$

$$\dot{W}_{in} = f\int (V \cdot I)dt = \frac{1}{2} V_0 I_0 \cos\phi_v \tag{4}$$

where, W_{in} is the electric input power (W) defined by Equation (4), V_0 is the peak voltage across the electric coil (V), I_0 is the peak current through the electric coil (A) and ϕ_v is the phase angle of the voltage relative to that of the current flow (°).

FURTHER IMPROVEMENT IN TWO WAYS

As discussed in the last section, the lowest temperature at the coldend was recorded to be 18.7 K at an operating frequency of 50 Hz. Can we say that the 'above results' are the best? The answer is definitely 'no'. Therefore, we have tried to improve the performance of the PTR in two ways as follows:

(i) Resonance matching between the thermal and mechanical systems

(ii) Regenerator optimization

For the first step, we need to analyze the physical variables (piston displacement and dynamic pressure amplitude) and whether the PTR properly operates near its resonance or not. In order to simulate the physical variables, a commercial software (SAGE) was used, as it considers the thermo-hydraulic governing equations for the working gas as well as the thermal properties of the solid

Table 2. Geometrical dimensions and operating parameters of the PTR system.

		Sim. data (i) & Exp. data	Sim. data (ii)
Linear compressor	Piston mass, m_p	235 g	260 g
	Mechanical stiffness, k_m	2,500 N m^{-1}	0 N m^{-1}
	Motor constant, K_E	4.8 N A^{-1}	
	Electric resistance, R_c	0.05 Ω	
	Electric inductance, L_c	1.9 mH	
Pulse tube components	Compression space	16,430 mm^3	
	Regenerator	22.2 mm (O.D.), 0.3 mm (T), 40 mm (H) *30 mm-portion; #400 stainless steel mesh (porosity: 0.65)* *10 mm-portion; 75 μm-diameter lead sphere (porosity: 0.35)*	
	Pulse tube	12.7 mm (O.D.), 0.3 mm (T), 75 mm (H)	
	Heat exchangers	Main rejecter: 9,600 mm^3; Secondary rejecter: 1,570 mm^3; Accepter: 1,310 mm^3	
	Phase controller	Inertance tube: 3.6 mm (I.D), 1.6 m (L); Reservoir: 500,000 mm^3	
Operating parameters	Operating temperature	Main rejecter: 80 K; Secondary rejecter: 90 K; Accepter: 20 K	
	Charging pressure	2 MPa	
	Input current	9.7 $A_{rms.}$	

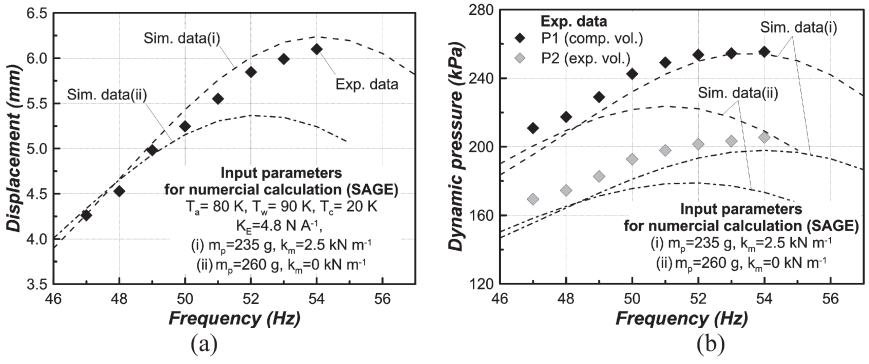

Figure 5. Comparison of (a) the piston displacement and (b) the dynamic pressure amplitude between the present results and the expected values with the linear compressor modifications

regenerator elements. The Sage model also includes the equations of motion (EOM) that describe the dynamic characteristics of the cold compressor's piston. As noted in the previous section, it seems that the frequency of 50 Hz (thermally best one) is not well matched to the compressor resonance when it is operated at cryogenic temperatures (its resonance is much higher than 50 Hz). At this point, we decided to reduce the natural frequency of the cold linear compressor by increasing the mass of the moving piston. Furthermore, it was determined that eliminating a flexure was advantageous for improving the compressor's mechanical reliability at cryogenic temperatures.

Table 2 shows the geometrical dimensions of the PTR system and the operating parameters. The values in the column 'Sim. data (i) & Exp. data' are designated for the apparatus currently constructed and tested in this research paper. The values for the further analysis with the modified compressor are listed in the last column 'Sim. data (ii).' Figure 5 shows a comparison of the piston displacement and the dynamic pressure amplitudes in the PTR system between the present results (both experimental and numerical) and the expected values with the proposed compressor modifications. The results obviously signify that the peak point is shifted from the 'high frequency region' to near 50 Hz.

Next, various methods can be pursued to characterize the regenerator thermo-hydraulic performance with its geometry and operating conditions. In this analysis, REGEN was adopted to analyze the thermal performance of the regenerator at the coldend with respect to the regenerative material

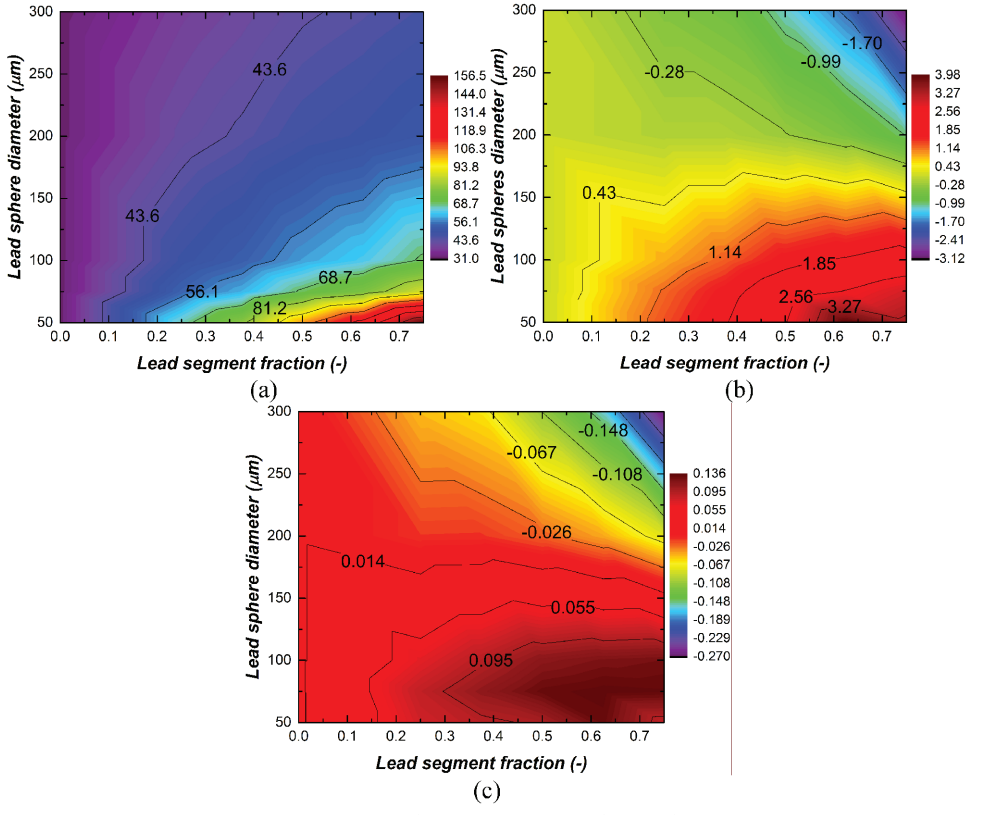

Figure 6. Performance maps of the multilayer regenerator with the fixed length of the regenerator (40 mm), (a) the required PV work at the warm-end of the regenerator, (b) the cooling power and (c) the COP of the PTR system

packing type. As mentioned in the previous section, the regenerator consists of two regenerative materials (stainless steel mesh screens and tiny lead spheres). Thus, the packing fraction and the particle size of each material should be optimized; this is especially true for the lead spheres. Also, the total length of the regenerator should be optimized. The optimization procedure was as follows:

(i) Determine the particle size of the lead spheres with the fixed regenerator length
(ii) Determine the total length of the regenerator with the selected size of the lead spheres

Since, as shown in the temperature distribution along the regenerator, Fig. 2(b), the thermal duty on the lead segment is exceedingly high relative to that of the total regenerator. Thus, the total amount of lead spheres should be increased beyond the current status. Table 3 lists the fixed and the controlling parameters for the optimization process. The fixed parameters, especially the mass flow rate, the pressure ratio, and the phase angle between them, are based on the computation results with the compressor modifications 'Sim. data (ii).' The operating frequency, therefore, is set to be 50 Hz. Figure 6 shows maps with respect to the particle size of the lead spheres and their portion (length fraction to the length of the regenerator of 40 mm). Figure 6(a) shows how much PV work is required at the warm-end of the regenerator when it operates with the input parameters tabulated in Table 3 and the specified geometric configurations. Figure 6(b) also presents the cooling power at the cold end of the regenerator. The cooling power includes auxiliary losses ($Q_{aux.\ losses}$) that the PTR system generates, i.e. shuttle heat transfer in the pulsating tube and conductive losses. Since we assume that the operating conditions are identical for all the calculations, the aforementioned losses can be roughly calculated [12]. The shuttle and the conduction thermal losses are estimated to be 0.96 W and 0.23 W, respectively. The COP is defined

Table 3. Operational parameters of regenerator (input parameters of REGEN).

Fixed parameter	Warm-end temperature, T_a (= temp. of the main rejecter)	80 K
	Cold-end temperature, T_c (= temp. of the accepter)	20 K
	Operating frequency, f	50 Hz
	Mean pressure, P_m	2 MPa
	Pressure ratio at the cold-end, $P_r=(P_m+P_2)/(P_m-P_2)$	1.2
	Inner diameter of regenerator, D_r	21.6 mm
	Mass flow rate at the cold-end, m_c	6 g s^{-1}
	Mass phase angle relative to that of the pressure at the cold end, $\square_{mP2}$	-15°
Controlling parameter	Particle size of the lead spheres	50~300 μm
	Length of the regenerator	40~70 mm
	Length fraction of the lead matrix to the total regenerator length	0~0.75

as the ratio of the effective cooling power (Q_c-$Q_{aux.\ losses}$) divided by the PV work at the warm-end of the regenerator and multiplied by the temperature ratio between them ($T_r=T_d/T_c$), as follows:.

$$COP = \frac{\dot{Q}_c - \dot{Q}_{aux.losses}}{\dot{W}_{PdV1}} T_r \tag{5}$$

From the map in Figure 6(c), which represents the coefficient of performance (COP), it appears that the 75 μm-diameter lead spheres tested in this paper was a good choice. As mentioned above, nevertheless, the map indicates the maximum COP when the length fraction of the lead matrix becomes approximately 60% (24 mm in equivalent length of the lead segment) not at 25% for the case of 40 mm-regenerator length. Although we did not measure the cooling power experimentally, the computation results predict that the current PTR system with some compressor modifications can achieve a cooling power level of 1.1 W with a COP of 0.087. Next, we have tried to optimize the length of the regenerator with the selected size of the lead sphere of 75 μm, as shown in Fig. 7.

Figure 7(c) clearly indicates the optimized regenerator dimension of 65 mm in length with the length fraction of the lead matrix of 40% (26 mm in equivalent length of the lead segment). The computation results also confirm that the equivalent length of the lead segment remains almost constant even if the total length of the regenerator is changed. As shown in Fig. 7(b), modifications, including further optimization on the regenerator length, can greatly enhance the cooling performance, i.e. a cooling power of 4.05 W with the COP of 0.17. From Fig. 7(a), we can also expect the input power of 119.5 W with the compression efficiency of 80%.

CONCLUSIONS

The development and test of a Stirling-type PTR system with a cold linear compressor has been discussed in this paper. We have tried to analyze the performance of the preliminary cold PTR system, and consequently an 'optimized system' has been suggested for maximizing its potential from the tested PTR system. The operational issues and main features regarding the Stirling-type PTR system are listed as follows.

(i) The cold linear compressor stably generates the mechanical work (PV work) at liquid nitrogen (LN_2) temperature.

(ii) The PV work at the compression space is indirectly deduced by a simple force phasor analysis. The resultant electrical to mechanical work conversion efficiency is estimated to exceed 80% for the entire frequency range.

(iii) The lowest temperature at the cold-end of the PTR system is recorded to be 18.7 K.

(iv) Through the dynamic analysis on the whole PTR system, the results obviously show that the peaks of the physical variables are shifted from the 'high frequency region' to near the target operating frequency of 50 Hz.

(v) For the lead matrix, the particle size of 75 μm-diameter is proper but its total amount should be increased to achieve the full potential of the PTR system.

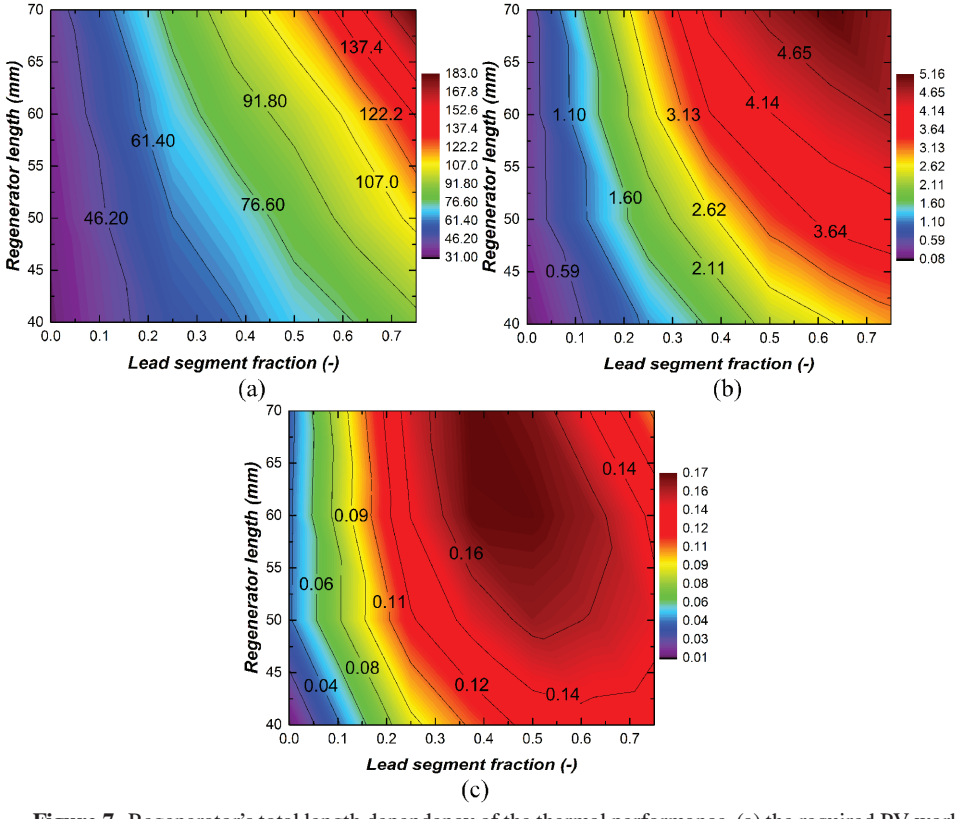

Figure 7. Regenerator's total length dependency of the thermal performance, (a) the required PV work at the warm-end of the regenerator, (b) the cooling power and (c) the COP of the PTR system.

With the modifications for both the cold linear compressor and the regenerator, an enhanced cooling performance, e.g.. cooling power of 4.1 W with the COP of 0.17, is expected. The overall experimental and analytical results signify that this 'piston-free colder expander' is viable and useful in many potential applications such as space and gas liquefaction industries.

ACKNOWLEDGMENT

This research was supported by the Converging Research Center Program through the Ministry of Science, ICT and Future Planning, Korea (2014M3C1A8048836). We also wish to thank National Institute of Standards and Technology (NIST) Cryogenics Technologies Group for providing REGEN3.3 program.

REFERENCES

1. J. M. Poncet, I. Charles, A. Gauthier, and T. Trollier, "Low Temperature High Frequency Pulse Tube Cooler Using Precooling," *Cryocoolers 13*, R. Ross, Jr., Ed., Springer US (2005), pp. 149-155.
2. G. Thummes, S. Bender, and C. Heiden, "Approaching the ^{4}He lambda line with a liquid nitrogen precooled two-stage pulse tube refrigerator," *Cryogenics,* vol. 36 (1996), pp. 709-711.
3. Z. Li, Y. Jiang, Z. Gan, L. Qiu, and J. Chen, "Performance of a precooled 4 K Stirling type high frequency pulse tube cryocooler with Gd_2O_2S," *Journal of Zhejiang University SCIENCE A,* vol. 15 (2014), pp. 508-516.
4. M. Dietrich and G. Thummes, "Two-stage high frequency pulse tube cooler for refrigeration at 25 K," *Cryogenics,* vol. 50 (2010), pp. 281-286.

5. Z. H. Gan, B. Y. Fan, Y. Z. Wu, L. M. Qiu, X. J. Zhang, and G. B. Chen, "A two-stage Stirling-type pulse tube cryocooler with a cold inertance tube," *Cryogenics,* vol. 50 (2010), pp. 426-431.

6. B. M. A. Cengel Y. A., *Thermodynamics*, 6 ed.: McGraw Hill, 2004.

7. E. Ercolani, J. M. Poncet, I. Charles, L. Duband, J. Tanchon, T. Trollier*, et al.*, "Design and prototyping of a large capacity high frequency pulse tube," *Cryogenics,* vol. 48 (2008), pp. 439-447.

8. M. Dietrich, L. W. Yang, and G. Thummes, "High-power Stirling-type pulse tube cryocooler: Observation and reduction of regenerator temperature-inhomogeneities," *Cryogenics,* vol. 47 (2007), pp. 306-314.

9. D. M. Sun, M. Dietrich, and G. Thummes, "High-power Stirling-type pulse tube cooler working below 30 K," *Cryogenics,* vol. 49 (2009), pp. 457-462.

10. T. Ki and S. Jeong, "Stirling-type pulse tube refrigerator with slit-type heat exchangers for HTS superconducting motor," *Cryogenics,* vol. 51 (2011), pp. 341-346.

11. T. Ki and S. Jeong, "Optimal design of the pulse tube refrigerator with slit-type heat exchangers," *Cryogenics,* vol. 50 (2010), pp. 608-614.

12. J. Jung and S. Jeong, "Surface Heat Pumping Loss in a Pulse Tube Refrigerator," *Cryocoolers 12*, R.G. Ross, Jr. Ed., Springer US (2003), pp. 371-378.